

Sensor and Simulation Notes

Note 263

31 May 1979

Excitation of the Parallel-Plate Section
of a Bounded-Wave EMP Simulator by a Conical Transmission Line

John Lam

Dikewood Industries, Inc.
Albuquerque, New Mexico 87106

Abstract

The excitation of a parallel-plate electromagnetic pulse (EMP) simulator by an electromagnetic pulser via a conical transmission line is analyzed. The analysis first establishes an exact formulation of the problem by use of the technique of electric-field integrodifferential equations. It then goes over to a simpler, approximate formulation in the form of an integrodifferential equation for the total longitudinal surface current flowing on the simulator. This equation is further transformed into an integral equation, and the modal structure of its solution investigated. A self-consistent method for solving the integral equation is developed. An analytical formula for the current in the transverse-electromagnetic (TEM) mode is thereby obtained. The analysis concludes with a numerical study of the TEM current and its variation with the parameters of the simulator geometry.

CLEARED FOR PUBLIC RELEASE

AFWL -TR- 79-136

263

264

265

2

Sensor and Simulation Notes

Note 263

31 May 1979

Excitation of the Parallel-Plate Section
of a Bounded-Wave EMP Simulator by a Conical Transmission Line

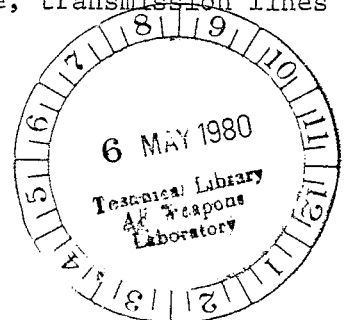
John Lam

Dikewood Industries, Inc.
Albuquerque, New Mexico 87106

Abstract

The excitation of a parallel-plate electromagnetic pulse (EMP) simulator by an electromagnetic pulser via a conical transmission line is analyzed. The analysis first establishes an exact formulation of the problem by use of the technique of electric-field integrodifferential equations. It then goes over to a simpler, approximate formulation in the form of an integrodifferential equation for the total longitudinal surface current flowing on the simulator. This equation is further transformed into an integral equation, and the modal structure of its solution investigated. A self-consistent method for solving the integral equation is developed. An analytical formula for the current in the transverse-electromagnetic (TEM) mode is thereby obtained. The analysis concludes with a numerical study of the TEM current and its variation with the parameters of the simulator geometry.

electric fields, electromagnetic pulse simulators, TEM mode, transmission lines



PREFACE

The author would like to thank Joe P. Martinez for performing the numerical computations of this work.

CONTENTS

<u>Section</u>		<u>Page</u>
I	INTRODUCTION	7
II	GEOMETRY	11
III	ELECTROMAGNETIC POTENTIALS	15
IV	EXACT FORMULATION	20
V	APPROXIMATE FORMULATION	23
VI	REDUCTION TO INTEGRAL EQUATION	26
VII	EVALUATION OF FOURIER TRANSFORMS	29
VIII	MODAL STRUCTURE OF EXCITATION	35
IX	SELF-CONSISTENT SOLUTION	38
X	NUMERICAL RESULTS	44
XI	DISCUSSIONS	49
	REFERENCES	50
	APPENDIX	51

ILLUSTRATIONS

<u>Figure</u>		<u>Page</u>
1	Typical Geometry of a Bounded-Wave EMP Simulator	8
2	Model for Studying the Junction in a Bounded-Wave EMP Simulator	9
3	Three-Dimensional Coordinate System for the Bounded-Wave Simulator Model	12
4	Two-Dimensional Coordinate System for the Surface of the Bounded-Wave Simulator Model	13
5	Division of the First Quadrant of the $\xi - \xi'$ Plane into Four Areas of Integration	30
6	Singularities in the Complex p -Plane	41

TABLES

<u>Table</u>		<u>Page</u>
1	Variation of Impedance Z_1 with Separation-to-Width Ratio h/a	45
2	Variation of Impedance Z_2 with Parameters kh and h/a	47
3	Variation of Impedance Z_3 with Parameters kh , h/a and L/h	48

SECTION I

INTRODUCTION

Bounded-wave electromagnetic-pulse (EMP) simulators utilize a pair of conductors to guide and confine the electromagnetic fields in the test volume. A portion of the conductors is often in the form of two parallel, rectangular plates or strips. Figure 1 shows a typical geometry of the bounded-wave simulator. It consists of two identical, long conductors joined together at one end to an electromagnetic pulser, and at the other end to a load termination. This conductor configuration can be regarded as made up of a section of a finite-width, parallel-plate transmission line sandwiched between two conical transmission lines. The test volume is located between the plates straddling the intersection of the input conical transmission line and the parallel plates.

When the pulser is fired, electric currents rush out from it onto the two conductors. These currents are accompanied by electromagnetic fields which propagate from the pulser toward the load. Because of the special geometrical design of the conductors, the electromagnetic fields will be predominantly in the transverse-electromagnetic (TEM) mode. This feature is highly desirable since the TEM mode closely resembles the plane-wave nature of the actual nuclear EMP. The load is suitably chosen to minimize reflection from the termination.

One approach to achieving an overall understanding of the performance of the bounded-wave simulator consists in isolating and analyzing specific aspects of the simulator operation. Such aspects include the electromagnetic propagation characteristics of the parallel-plate and conical transmission lines. These have been studied in references 1, 2 and 3. Another aspect of special importance is the propagation of the electromagnetic excitation from the conical transmission line onto the parallel plates. The manner of transition of the excitation across the junction directly affects the electromagnetic fields in the test volume.

This report presents a theoretical study of the simulator junction. The analysis is based on a geometrical model shown in figure 2. The model consists of a semi-infinite section of a parallel-plate transmission line

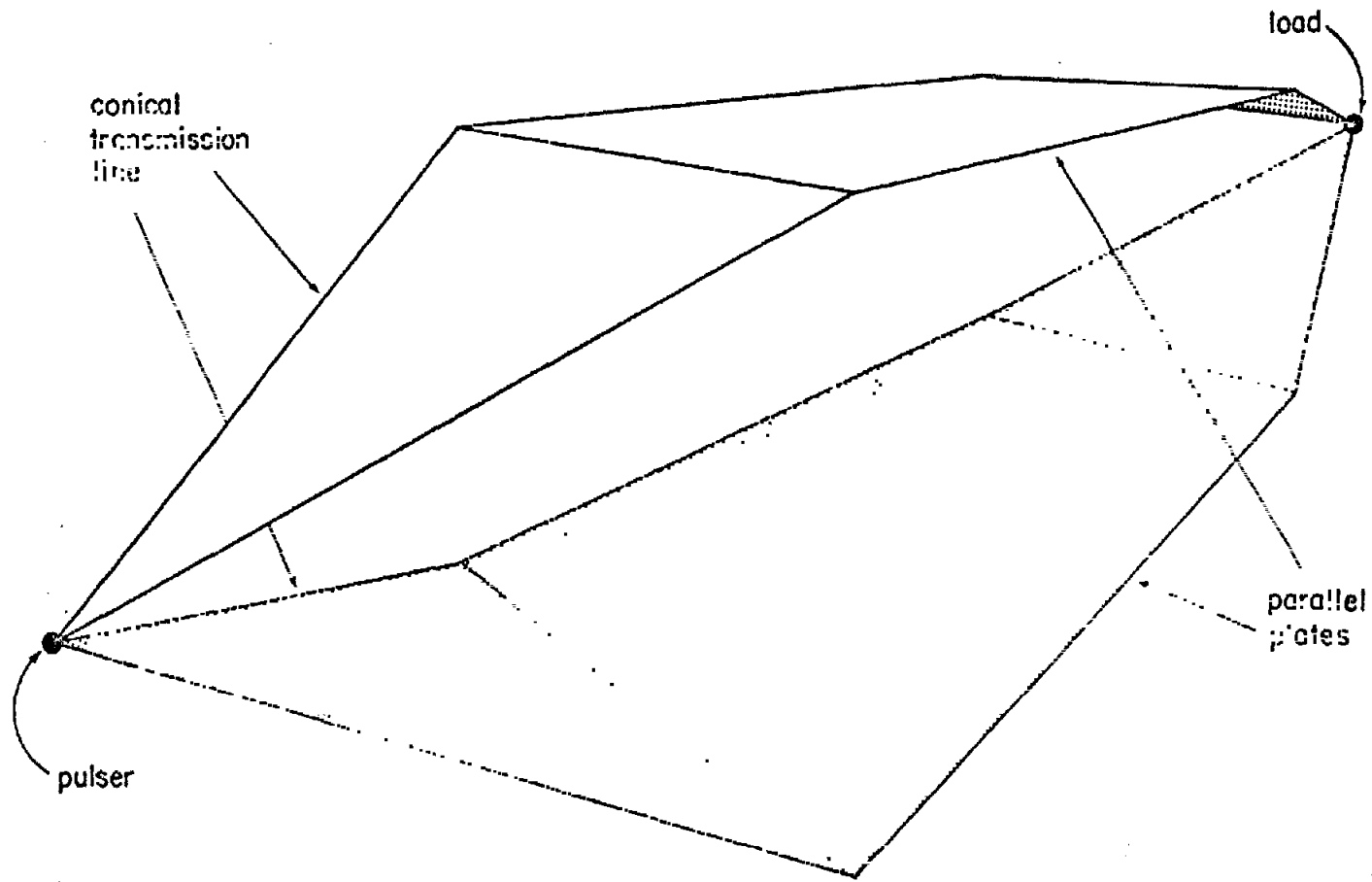


Figure 1. Typical Geometry of a Bounded-Wave EMP Simulator.

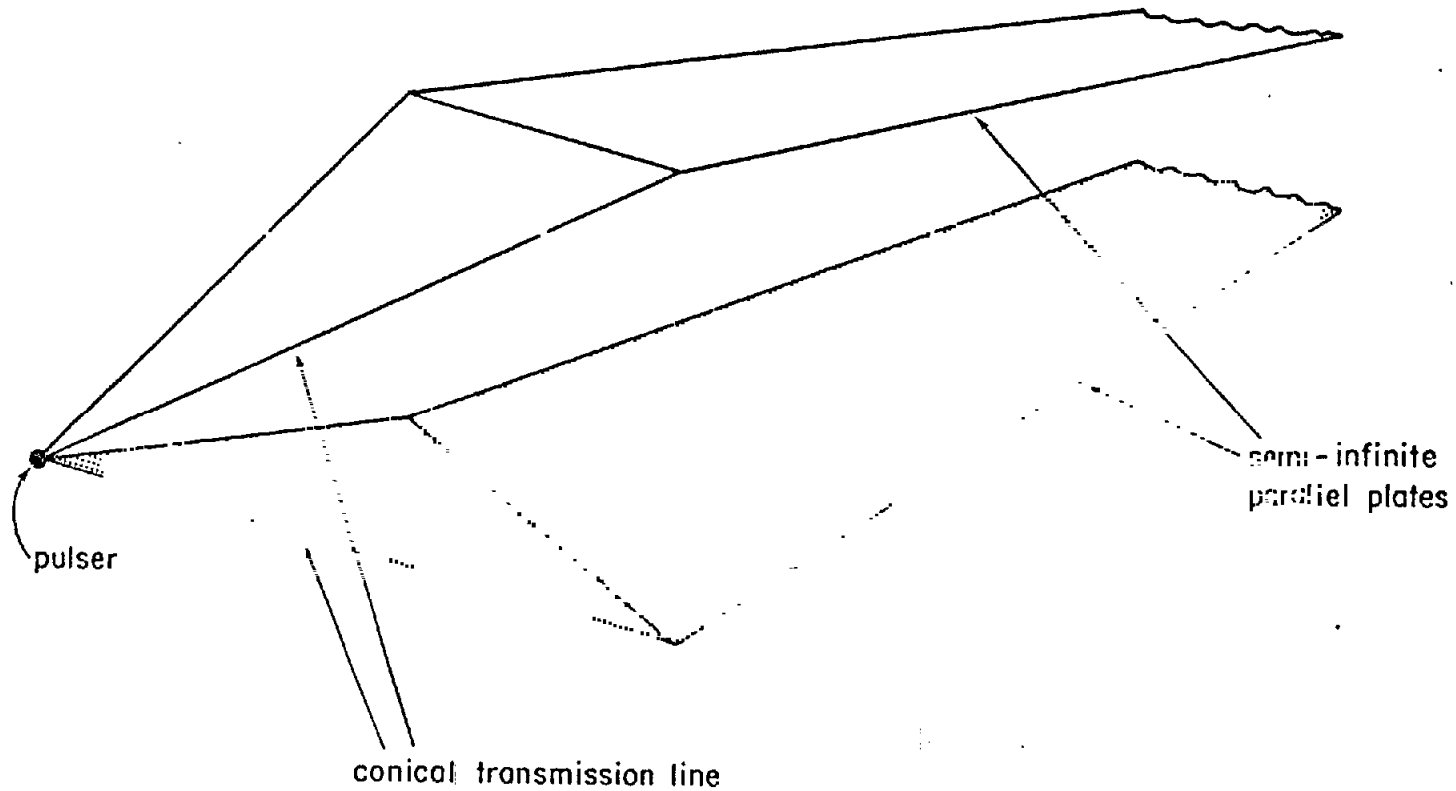


Figure 2. Model for Studying the Junction in a Bounded-Wave EMP Simulator.

connected to a finite section of a conical transmission line. Both transmission lines are assumed to be made out of infinitely thin and perfectly conducting sheets. The conical transmission line is excited at the apex by a given pulser. It is required to calculate the resulting electromagnetic excitation propagating onto the parallel-plate section.

The model clearly reproduces exactly the geometry of the pulser end of the simulator. One has, however, exploited the weakness of the reflection from the termination to replace the load end with a semi-infinite continuation of the parallel-plate section. The geometry becomes sufficiently simple to permit an approximate analytical solution.

SECTION II

GEOMETRY

In studying the bounded-wave simulator model of figure 2, it is mathematically convenient to consider instead an equivalent model consisting of a single conductor over an infinite, conducting ground plane. The image of the conductor below the ground plane replaces the second conductor. The apex of the conductor in this equivalent model is to be driven against the ground plane by an equivalent pulser.

One sets up a rectangular coordinate system such that the x-y plane coincides with the conducting ground plane, as shown in figure 3. Let the conductor be situated in the upper half-space $z > 0$. Its apex is located at the coordinate origin. Its semi-infinite-strip section is parallel to the ground plane along the positive x-axis. Let the width of the strip be denoted by $2a$ and its height above the ground plane by h . The conical section is actually an isosceles triangle of height d and base length $2a$. It is inclined to the ground plane at an angle θ such that

$$\sin \theta = \frac{h}{d} \quad (1)$$

It will be convenient to introduce at the same time a two-dimensional rectangular coordinate system on the surface of the conductor itself. In this system a point on the conductor is uniquely defined by a pair of coordinates (ξ, y) , as shown in figure 4. Here y is the same as the y-coordinate of the three-dimensional rectangular coordinate system, while ξ is related to x and z by linear relations. Let the triangular plate be denoted by S_1 and the strip by S_2 . The entire surface of the conductor will be denoted by $S (= S_1 + S_2)$. Then these linear relations are:

1. On S_1 ($0 < \xi < d$)

$$x = \xi \cos \theta \quad (2)$$

$$z = \xi \sin \theta$$

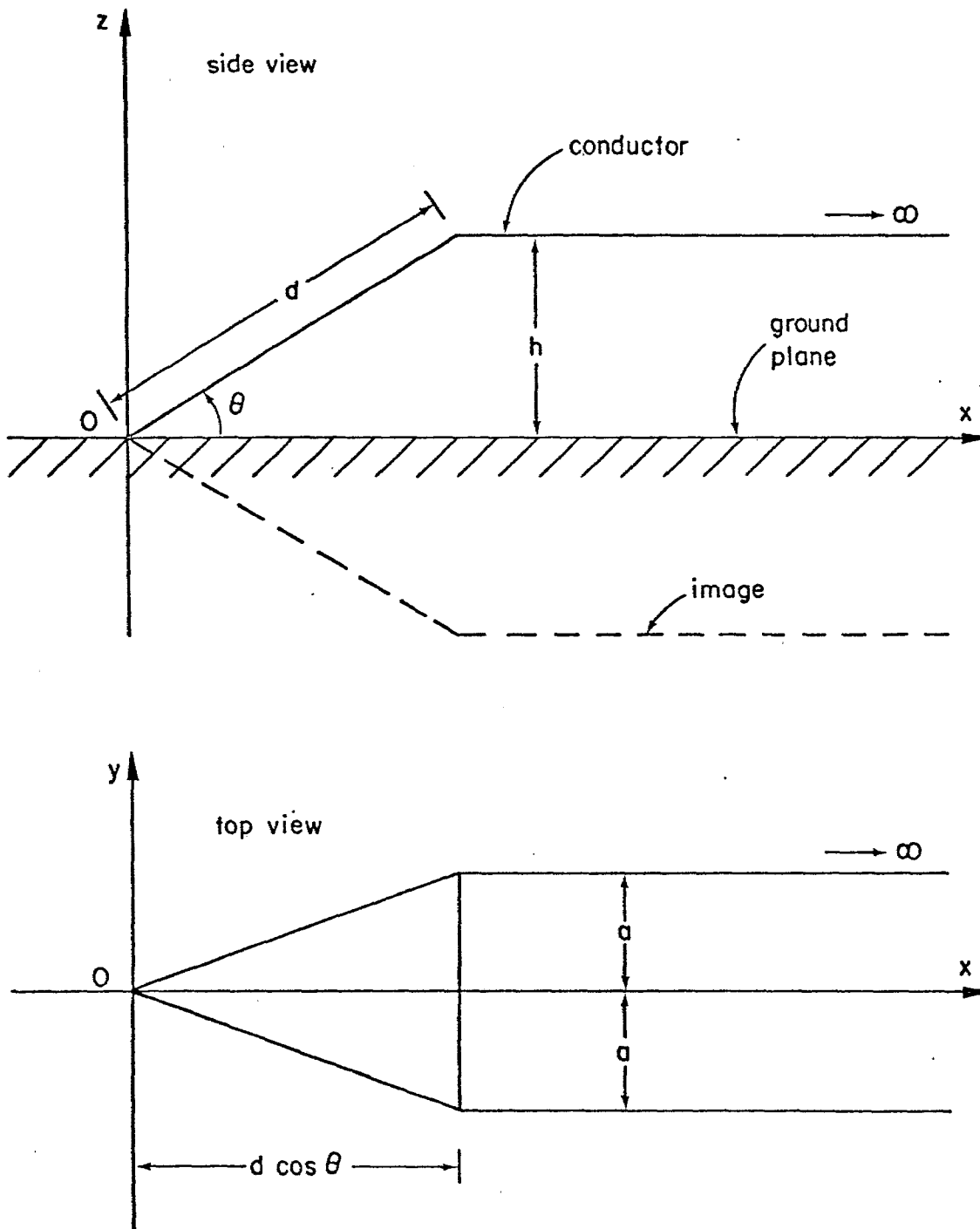


Figure 3. Three-Dimensional Coordinate System for the Bounded-Wave Simulator Model.

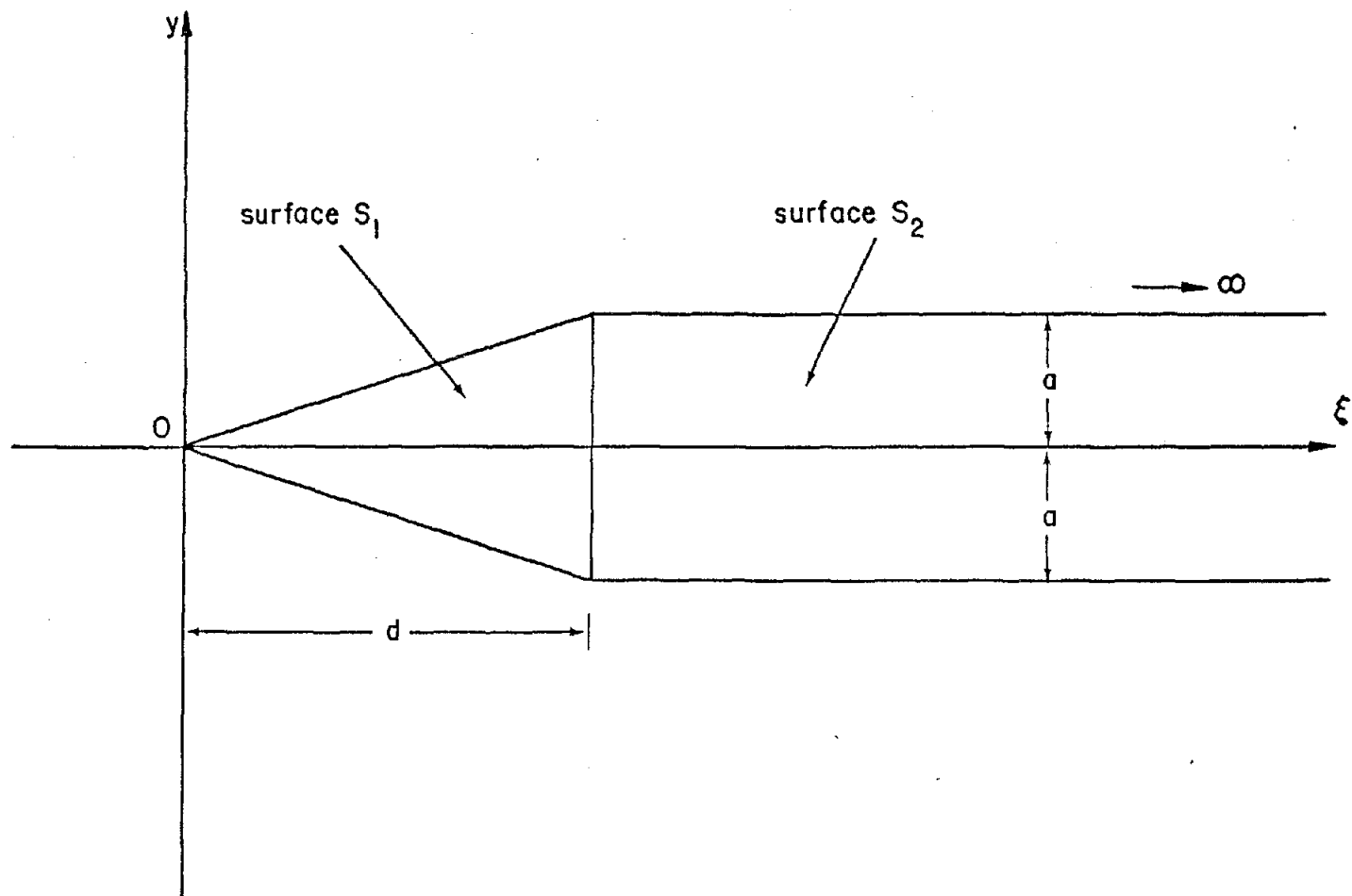


Figure 4. Two-Dimensional Coordinate System for the Surface of the Bounded-Wave Simulator Model.

2. On S_2 ($d < \xi < \infty$)

$$x = \xi - d + d \cos \theta \quad (3)$$

$$z = h$$

One may call ξ the longitudinal coordinate and y the transverse coordinate.

Note that the apex of the conductor is situated at $\xi = y = 0$.

SECTION III
ELECTROMAGNETIC POTENTIALS

The bounded-wave simulator model of figure 3 can be analyzed in the frequency domain. One considers the pulser as a time-harmonic voltage source driving the apex of the conductor against the ground. Its variation with time t is described by the time factor $e^{j\omega t}$ with angular frequency ω . For simplicity it will be assumed that ω is positive. Results corresponding to negative ω can be obtained from those for positive ω by complex conjugation. Under this excitation a time-harmonic electric current flows on the conductor as well as on the ground. It suffices for the analysis to calculate the surface current density on the conductor.

In this study the current on the conductor will be calculated by using the electric-field integrodifferential equation. This approach has great methodological appeal in that it enables one to obtain an exact formulation of the problem, despite the difficult geometry of the conductor. This exact formulation serves as a solid base from which approximations can safely proceed. The idea of the formulation is to relate the electric field outside the conductor to the current on the conductor, and then impose boundary conditions on the electric field at the surface of the conductor. For this purpose it is convenient to introduce the electromagnetic potentials.

Let \underline{r} denote a point in the upper half-space $z > 0$:

$$\underline{r} = (x, y, z) \tag{4}$$

and let $\underline{E}(\underline{r})$ and $\underline{B}(\underline{r})$ be the electromagnetic fields at \underline{r} generated by the currents and charges on the conductor and the ground plane. Then \underline{E} and \underline{B} can be derived from a pair of scalar and vector electromagnetic potentials $\varphi(\underline{r})$ and $\underline{A}(\underline{r})$:

$$\underline{E}(\underline{r}) = -\nabla \varphi(\underline{r}) - j\omega \underline{A}(\underline{r}) \tag{5}$$

$$\underline{B}(\underline{r}) = \nabla \times \underline{A}(\underline{r})$$

In the Lorentz gauge these potentials individually satisfy the Helmholtz equation:

$$(\nabla^2 + k^2)\varphi(\underline{r}) = 0 \quad (6)$$

$$(\nabla^2 + k^2)\underline{A}(\underline{r}) = 0$$

where

$$k = \omega\sqrt{\epsilon_0\mu_0} \quad (7)$$

and ϵ_0 and μ_0 are the permittivity and permeability of free space. By use of suitable Green's functions the solutions of equations 6 can be represented as integrals over the surface charge density σ and the surface current density \underline{K} on the surface S of the conductor alone:

$$\begin{aligned} \varphi(\underline{r}) &= \frac{1}{\epsilon_0} \int_S G_D(\underline{r}, \underline{r}') \sigma(\underline{r}') dS' \\ A_x(\underline{r}) &= \mu_0 \int_S G_D(\underline{r}, \underline{r}') K_x(\underline{r}') dS' \\ A_y(\underline{r}) &= \mu_0 \int_S G_D(\underline{r}, \underline{r}') K_y(\underline{r}') dS' \\ A_z(\underline{r}) &= \mu_0 \int_S G_N(\underline{r}, \underline{r}') K_z(\underline{r}') dS' \end{aligned} \quad (8)$$

In these expressions \underline{r}' denotes a point on the surface S :

$$\underline{r}' = (x', y', z') \quad (9)$$

and dS' is a surface element of S at \underline{r}' .

The functions G_D and G_N are Green's functions of the Helmholtz equation in the half-space $z > 0$:

$$\begin{aligned} (\nabla^2 + k^2)G_D(\underline{r}, \underline{r}') &= -\delta^3(\underline{r} - \underline{r}') \\ (\nabla^2 + k^2)G_N(\underline{r}, \underline{r}') &= -\delta^3(\underline{r} - \underline{r}') \end{aligned} \quad (10)$$

They satisfy, respectively, the homogeneous Dirichlet and Neumann boundary conditions on the ground plane $z = 0$:

$$\begin{aligned} G_D(\underline{r}, \underline{r}') &= 0 \\ \frac{\partial}{\partial z} G_N(\underline{r}, \underline{r}') &= 0 \end{aligned} \tag{11}$$

By introducing the image \underline{r}'' of \underline{r}' with respect to the ground plane, such that

$$\underline{r}'' = (x', y', -z') \tag{12}$$

one can construct G_D and G_N from the free-space Green's function G_0 :

$$G_0(\underline{r}, \underline{r}') = \frac{e^{-jk|\underline{r} - \underline{r}'|}}{4\pi|\underline{r} - \underline{r}'|} \tag{13}$$

The results are:

$$\begin{aligned} G_D(\underline{r}, \underline{r}') &= G_0(\underline{r}, \underline{r}') - G_0(\underline{r}, \underline{r}'') \\ G_N(\underline{r}, \underline{r}') &= G_0(\underline{r}, \underline{r}') + G_0(\underline{r}, \underline{r}'') \end{aligned} \tag{14}$$

The free-space Green's function G_0 in equation 13 already has a simple, closed form. Nevertheless, in later calculations, it will be advantageous to work also with its Fourier-integral representation:

$$G_0(\underline{r}, \underline{r}') = \frac{1}{(2\pi)^3} \int_{-\infty}^{\infty} d\alpha \int_{-\infty}^{\infty} d\beta \int_{-\infty}^{\infty} d\gamma \frac{e^{-j[\alpha(x-x') + \beta(y-y') + \gamma(z-z')]}}{\alpha^2 + \beta^2 + \gamma^2 - k^2} \tag{15}$$

For this expression to be identical to equation 13, it must be understood that k has an infinitesimal, negative imaginary part:

$$k \rightarrow k - j\epsilon \quad \epsilon > 0 \tag{16}$$

The surface integrals in equations 8 take on a simpler form if one goes over from the three-dimensional coordinate system (x,y,z) to the two-dimensional coordinate system (ξ,y) set up on the conductor's surface S , as defined in equations 2 and 3. In the latter coordinate system the surface current density \underline{K} has only two components K_ξ and K_y . The components K_x and K_z in the former coordinate system are both related to K_ξ .

1. On S_1

$$K_x = K_\xi \cos \theta \quad (17)$$

$$K_z = K_\xi \sin \theta$$

2. On S_2

$$K_x = K_\xi \quad (18)$$

$$K_z = 0$$

In terms of K_ξ and K_y , the vector potential \underline{A} reads

$$A_x(\underline{r}) = \mu_0 \int_{S_1} G_D(\underline{r}, \underline{r}') \cos \theta K_\xi(\underline{r}') dS' + \mu_0 \int_{S_2} G_D(\underline{r}, \underline{r}') K_\xi(\underline{r}') dS'$$

$$A_y(\underline{r}) = \mu_0 \int_S G_D(\underline{r}, \underline{r}') K_y(\underline{r}') dS' \quad (19)$$

$$A_z(\underline{r}) = \mu_0 \int_{S_1} G_N(\underline{r}, \underline{r}') \sin \theta K_\xi(\underline{r}') dS'$$

In these expressions the components of \underline{r}' are related to the source coordinates (ξ', y') according to equations 2 and 3, while

$$dS' = d\xi' dy' \quad (20)$$

The surface charge density σ is related to the surface current density \underline{K} through the equation of continuity:

$$\begin{aligned} -j\omega\sigma(\underline{r}') &= \nabla' \cdot \underline{K}(\underline{r}') \\ &= \frac{\partial}{\partial \xi'} K_{\xi}(\underline{r}') + \frac{\partial}{\partial y'} K_y(\underline{r}') \end{aligned} \quad (21)$$

By use of this relation one can eliminate σ from further consideration. The expression for the scalar potential then becomes

$$\varphi(\underline{r}) = \frac{-1}{j\omega\epsilon_0} \int_S G_D(\underline{r}, \underline{r}') \nabla' \cdot \underline{K}(\underline{r}') dS' \quad (22)$$

SECTION IV
EXACT FORMULATION

There are two electric-field integrodifferential equations for this problem. They are formulated by imposing appropriate boundary conditions on the two tangential components $E_\xi(\underline{r})$ and $E_y(\underline{r})$ of the electric field at every point \underline{r} on the conductor's surface S . To derive these boundary conditions one regards the pulser as the supplier and maintainer of a definite tangential electric field with components $E_\xi^0(\underline{r})$ and $E_y^0(\underline{r})$ on the conductor. One then requires that $E_\xi(\underline{r})$ and $E_y(\underline{r})$ assume these prescribed values on S , that is,

$$E_\xi(\underline{r}) = E_\xi^0(\underline{r}) \tag{23}$$

$$E_y(\underline{r}) = E_y^0(\underline{r})$$

for \underline{r} lying on S .

In its idealized form the pulser is a localized voltage source. It generates a finite, time-harmonic voltage V_0 across the infinitesimal gap between the two triangular plates at the apex of the conical transmission line in figure 2. The tangential components of the pulser electric field are therefore given by

$$E_\xi^0(\underline{r}) = -V_0 \delta(\xi) \tag{24}$$

$$E_y^0(\underline{r}) = 0$$

The δ -function is normalized to make

$$\int_{-\infty}^{\infty} d\xi \delta(\xi) = 1 \tag{25}$$

Therefore the voltage across the apex of the conductor and the ground plane in figure 4 is $\frac{1}{2} V_0$ since

$$- \int_0^{\infty} d\xi E_{\xi}^0(\underline{r}) = \frac{1}{2} V_0 \quad (26)$$

The integration over ξ from 0 to ∞ picks up only one half of the contribution from the δ -function in E_{ξ}^0 .

Combining equations 5, 23 and 24 one obtains the following pair of boundary conditions for the potentials:

$$\frac{\partial}{\partial \xi} \varphi(\underline{r}) + j\omega A_{\xi}(\underline{r}) = V_0 \delta(\xi) \quad (27)$$

$$\frac{\partial}{\partial y} \varphi(\underline{r}) + j\omega A_y(\underline{r}) = 0$$

for \underline{r} lying on S . The component A_{ξ} is related to A_x and A_z as follows:

1. On S_1

$$A_{\xi} = A_x \cos \theta + A_z \sin \theta \quad (28)$$

2. On S_2

$$A_{\xi} = A_x \quad (29)$$

Substituting equations 28 and 29 into equations 27 and eliminating the potentials by use of equations 19 and 22, one transforms the boundary conditions into a pair of coupled integrodifferential equations for the two components K_{ξ} and K_y of the surface current density:

$$\begin{aligned} \frac{\partial}{\partial \xi} \int_S G_D(\underline{r}, \underline{r}') \nabla' \cdot \underline{K}(\underline{r}') dS' + k^2 \int_S G_H(\underline{r}, \underline{r}') K_{\xi}(\underline{r}') dS' \\ = - j\omega \epsilon_0 V_0 \delta(\xi) \end{aligned} \quad (30)$$

$$\frac{\partial}{\partial y} \int_S G_D(\underline{r}, \underline{r}') \nabla' \cdot \underline{K}(\underline{r}') dS' + k^2 \int_S G_D(\underline{r}, \underline{r}') K_y(\underline{r}') dS' = 0$$

The quantity $G_H(\underline{r}, \underline{r}')$ is a hybrid Green's function. It is a linear combination of the Dirichlet and Neumann Green's functions G_D and G_N , and is defined in the following manner:

1. For \underline{r} and \underline{r}' on S_1

$$G_H(\underline{r}, \underline{r}') = G_D(\underline{r}, \underline{r}') \cos^2 \theta + G_N(\underline{r}, \underline{r}') \sin^2 \theta \quad (31)$$

2. For \underline{r} on S_1 and \underline{r}' on S_2 , or vice versa

$$G_H(\underline{r}, \underline{r}') = G_D(\underline{r}, \underline{r}') \cos \theta \quad (32)$$

3. For \underline{r} and \underline{r}' on S_2

$$G_H(\underline{r}, \underline{r}') = G_D(\underline{r}, \underline{r}') \quad (33)$$

Equations 30 are in part differential equations. They must be supplemented by additional boundary conditions. These can be taken as the requirement that the components of the surface current density normal to the edges of the conductor be zero. On S_1 the edges are given by $y = \pm(a/d)\xi$. On S_2 they are given by $y = \pm a$. The boundary conditions on these edges are:

1. On S_1

$$K_y = \pm \frac{a}{d} K_\xi \quad \text{for } y = \pm \frac{a}{d} \xi \quad (34)$$

2. On S_2

$$K_y = 0 \quad \text{for } y = \pm a \quad (35)$$

The integrodifferential equations 30 and the boundary conditions 34 and 35 provide an exact formulation of the bounded-wave simulator model of figure 2.

SECTION V

APPROXIMATE FORMULATION

Equations 30 are a pair of coupled, two-dimensional, partial integro-differential equations. Their solution constitutes a formidable mathematical problem. At the moment it does not appear possible to forge ahead with the solution without introducing approximations. In the following calculations a number of approximations will be made. They enable one to obtain an approximate solution of the problem in analytical form.

One type of approximation to be applied is aimed at simplifying the basic equations of the problem. What one essentially does is to smooth out the transverse variations of the surface current density by an averaging process. In this way one is led to an approximate integrodifferential equation for the total longitudinal current flowing on the conductor. This equation constitutes an approximate formulation of the bounded-wave simulator problem.

Consider the first member of the two basic equations 30

$$\begin{aligned} & \frac{\partial}{\partial \xi} \int_0^{\infty} d\xi' \int_{-\lambda(\xi')}^{\lambda(\xi')} dy' G_D(\xi, y, \xi', y') \left[\frac{\partial}{\partial \xi'} K_{\xi}(\xi', y') + \frac{\partial}{\partial y'} K_y(\xi', y') \right] \\ & + k^2 \int_0^{\infty} d\xi' \int_{-\lambda(\xi')}^{\lambda(\xi')} dy' G_H(\xi, y, \xi', y') K_{\xi}(\xi', y') = -j\omega\epsilon_0 V_0 \delta(\xi) \end{aligned} \quad (36)$$

The quantity $\lambda(\xi')$ appearing in the limits of the y' -integration is defined as follows:

$$\lambda(\xi') = \begin{cases} a\xi'/d & 0 < \xi' < d \\ a & d < \xi' < \infty \end{cases} \quad (37)$$

The difference in the functional form of $\lambda(\xi')$ for the two ranges of ξ' reflects the fact that for $\xi' < d$ the conductor is a triangular plate, while

for $\xi' > d$ it is a rectangular strip. The left-hand side of equation 36 is proportional to the ξ -component of the electric field on the conductor generated by the surface current and charge densities on the conductor. The kernels G_D and G_H can be regarded as coupling functions relating the surface current and charge densities at the source point (ξ', y') to the longitudinal component of the electric field at the field point (ξ, y) . One can extract from equation 36 an approximate equation for the total longitudinal current by first neglecting the transverse surface current density K_y and then averaging out the dependences in the two kernels G_D and G_H on the transverse coordinates y and y' .

The two specific approximations can be justified on the ground that one has under consideration a very long conductor which is driven at one end by a voltage source. In this situation the surface current will be flowing predominantly in the longitudinal direction. One can expect the following inequality to hold generally:

$$|K_\xi| \gg |K_y| \quad (38)$$

The discarding of K_y from equation 36 will therefore incur only a small error. Furthermore, precisely because the conductor is long, it will be a good approximation to replace the two coupling functions G_D and G_H by their averages in the transverse direction. That is to say, one lets

$$G_D(\xi, y, \xi', y') \rightarrow \Gamma_D(\xi, \xi') = \frac{1}{4\lambda(\xi)\lambda(\xi')} \int_{-\lambda(\xi)}^{\lambda(\xi)} dy \int_{-\lambda(\xi')}^{\lambda(\xi')} dy' G_D(\xi, y, \xi', y') \quad (39)$$

and

$$G_H(\xi, y, \xi', y') \rightarrow \Gamma_H(\xi, \xi') = \frac{1}{4\lambda(\xi)\lambda(\xi')} \int_{-\lambda(\xi)}^{\lambda(\xi)} dy \int_{-\lambda(\xi')}^{\lambda(\xi')} dy' G_H(\xi, y, \xi', y') \quad (40)$$

In this way equation 36 becomes an ordinary integrodifferential equation for the total longitudinal current $I(\xi)$:

$$\frac{d}{d\xi} \int_0^{\infty} d\xi' \Gamma_D(\xi, \xi') \frac{d}{d\xi'} I(\xi') + k^2 \int_0^{\infty} d\xi' \Gamma_H(\xi, \xi') I(\xi') = -j\omega\epsilon_0 V_0 \delta(\xi) \quad (41)$$

where

$$I(\xi) = \int_{-\lambda(\xi)}^{\lambda(\xi)} dy K_{\xi}(\xi, y) \quad (42)$$

Equation 41 is a closed equation for the total longitudinal current. Although by no means trivial, it is significantly simpler than the pair of exact equations 30. The calculations in the following sections will be based on this approximate formulation of the bounded-wave simulator problem.

SECTION VI

REDUCTION TO INTEGRAL EQUATION

The integrodifferential equation 41 can be reduced to a pure integral equation by Fourier transformation. Introduce the double Fourier sine and cosine transforms F_D and F_H of the kernels Γ_D and Γ_H :

$$F_D(p, p') = \left(\frac{2}{\pi}\right)^2 \int_0^\infty d\xi \int_0^\infty d\xi' \Gamma_D(\xi, \xi') \sin p\xi \sin p'\xi' \quad (43)$$

$$F_H(p, p') = \left(\frac{2}{\pi}\right)^2 \int_0^\infty d\xi \int_0^\infty d\xi' \Gamma_H(\xi, \xi') \cos p\xi \cos p'\xi'$$

The inverse transforms are

$$\Gamma_D(\xi, \xi') = \int_0^\infty dp \int_0^\infty dp' F_D(p, p') \sin p\xi \sin p'\xi' \quad (44)$$

$$\Gamma_H(\xi, \xi') = \int_0^\infty dp \int_0^\infty dp' F_H(p, p') \cos p\xi \cos p'\xi'$$

Substituting equations 44 into equation 41, one obtains

$$\begin{aligned} \frac{d}{d\xi} \int_0^\infty dq \int_0^\infty dp' F_D(q, p') \sin q\xi P(p') + k^2 \int_0^\infty dq \int_0^\infty dp' F_H(q, p') \cos q\xi Q(p') \\ = -j\omega\epsilon_0 V_0 \delta(\xi) \end{aligned} \quad (45)$$

where

$$\begin{aligned} P(p') &= \int_0^\infty d\xi' \sin p'\xi' \frac{d}{d\xi'} I(\xi') \\ Q(p') &= \int_0^\infty d\xi' \cos p'\xi' I(\xi') \end{aligned} \quad (46)$$

For these two integrals to exist one must assume that the conductor is slightly resistive, so that the total current I and its derivatives vanish at infinity.

Next, multiply both sides of equation 45 by $\cos p\xi$ and integrate over ξ from 0 to ∞ . The operator $d/d\xi$ can be handled by integration by parts. Then, making use of the identities

$$\frac{2}{\pi} \int_0^{\infty} d\xi \sin p\xi \sin p'\xi = \delta(p - p') \quad (47)$$

$$\frac{2}{\pi} \int_0^{\infty} d\xi \cos p\xi \cos p'\xi = \delta(p - p')$$

valid for $p, p' > 0$, one obtains

$$\int_0^{\infty} dp' \left[pF_D(p, p')P(p') + k^2 F_H(p, p')Q(p') \right] = - \frac{j\omega\epsilon_0 V_0}{\pi} \quad (48)$$

The two functions P and Q are closely related to the Fourier cosine transform $A(p)$ of the total current I :

$$A(p) = \frac{2}{\pi} \int_0^{\infty} d\xi I(\xi) \cos p\xi \quad (49)$$

with the inverse transform

$$I(\xi) = \int_0^{\infty} dp A(p) \cos p\xi \quad (50)$$

From equations 46 one easily sees that

$$P(p') = - \frac{\pi}{2} p'A(p') \quad (51)$$

$$Q(p') = \frac{\pi}{2} A(p')$$

Therefore, substituting equations 51 into equation 48, one obtains

$$\int_0^{\infty} dp' \left[-pp'F_D(p, p') + k^2 F_H(p, p') \right] A(p') = - \frac{2j\omega\epsilon_0 V_0}{\pi^2} \quad (52)$$

Equation 52 has the appearance of a Fredholm integral equation of the first kind for the unknown function $A(p')$. Actually it is an integral equation of the second kind. In the following section it will be shown that both F_D and F_H in the kernel contain a δ -function:

$$\begin{aligned} F_D(p,p') &= \rho(p)\delta(p-p') + f_D(p,p') \\ F_H(p,p') &= \rho(p)\delta(p-p') + f_H(p,p') \end{aligned} \quad (53)$$

The coefficient of the δ -function is the same in both cases. Upon substitution of equations 53 into equation 52, the latter becomes

$$(k^2 - p^2)\rho(p)A(p) + \int_0^\infty dp' \Lambda(p,p')A(p') = - \frac{2j\omega\epsilon_0 V_0}{\pi^2} \quad (54)$$

where the new kernel $\Lambda(p,p')$ is given by

$$\Lambda(p,p') = k^2 f_H(p,p') - pp' f_D(p,p') \quad (55)$$

Equation 54 is an exact consequence of equation 41. Being essentially an integral equation of the second kind, it is a convenient starting point for constructing an approximate analytical solution.

SECTION VII

EVALUATION OF FOURIER TRANSFORMS

Before proceeding with the solution of equation 54, it is necessary to obtain explicit expressions for the two quantities $\rho(p)$ and $\Lambda(p,p')$. This is done by calculating the double Fourier transforms $F_D(p,p')$ and $F_H(p,p')$ defined in equations 43.

The evaluation of the two double integrals in equations 43 is complicated by the fact that the kernels $\Gamma_D(\xi,\xi')$ and $\Gamma_H(\xi,\xi')$ have different functional dependences on their arguments over different parts of the domain of integration. This situation can be appreciated by examining the $\xi - \xi'$ plane in figure 5. The double integrals are over the first quadrant of the plane. This quadrant has been divided into four areas labeled 1,2,3 and 4, with the boundaries located at $\xi = d$ and $\xi' = d$. Across these boundaries the functional relations between (x,z) and ξ , and between (x',z') and ξ' , undergo a change according to equations 2 and 3. The change produces a corresponding discontinuity in the functional forms of Γ_D and Γ_H . This discontinuity is of course a reflection of the geometrical discontinuity at the junction of the triangular plate and the rectangular strip.

The kernels $\Gamma_D(\xi,\xi')$ and $\Gamma_H(\xi,\xi')$ can be regarded as averaged coupling functions between the field point at ξ and the source point at ξ' . Area 1 in figure 5 corresponds to the situation in which both the field point and the source point are on the triangular plate S_1 , while area 2 corresponds to that in which they are both on the rectangular strip S_2 . For areas 3 and 4 the two points are on different sections of the conductor.

Of the four areas, area 2 is the most important, being the most extensive. By equation 33 Γ_D and Γ_H are identical in area 2:

$$\Gamma_D(\xi,\xi') = \Gamma_H(\xi,\xi') = W(\xi - \xi') \quad \text{for } \xi, \xi' > d \quad (56)$$

By equations 14, 39 and 40, one has

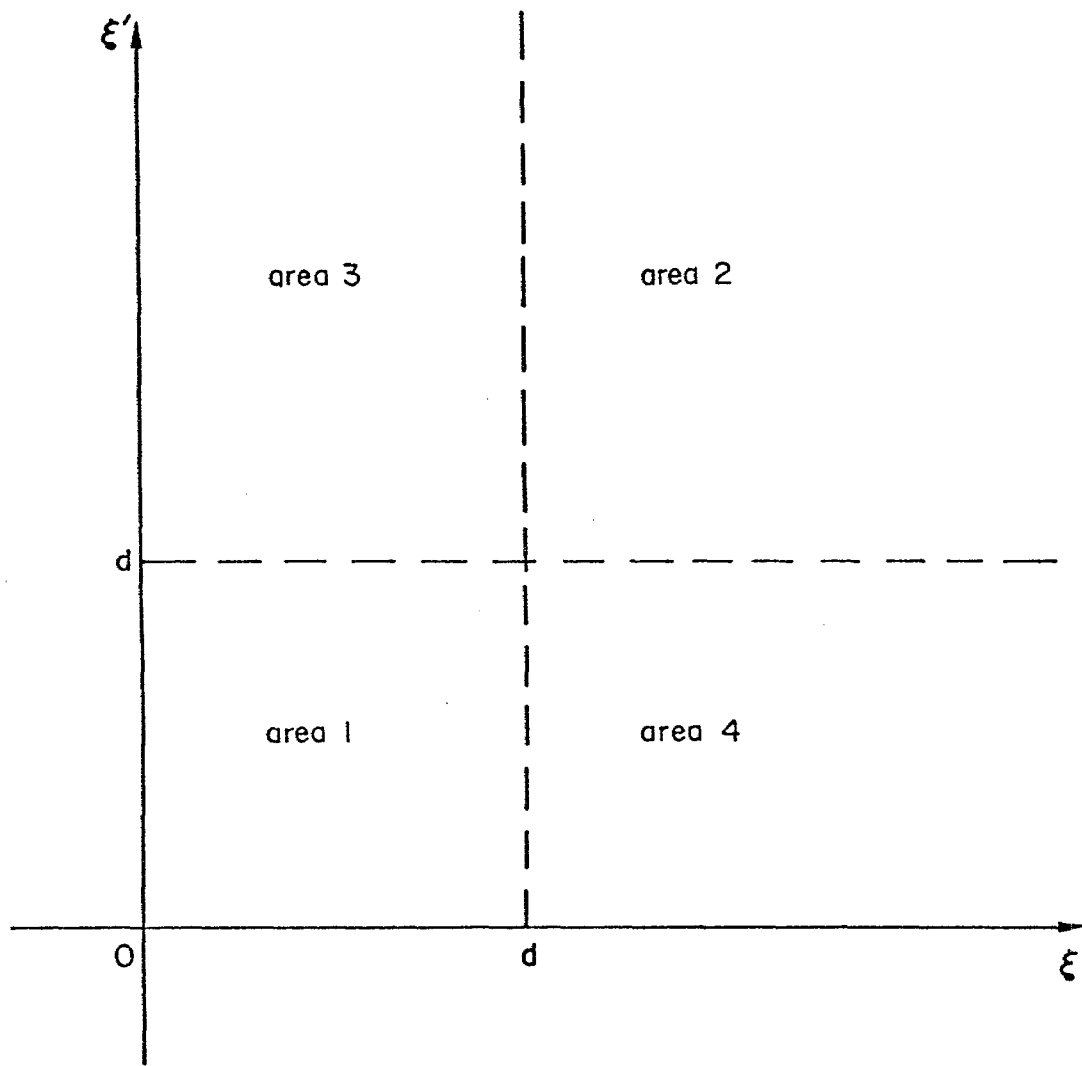


Figure 5. Division of the First Quadrant of the $\xi - \xi'$ Plane into Four Areas of Integration.

$$W(\xi - \xi') = \frac{1}{4a^2} \int_{-a}^a dy \int_{-a}^a dy' \frac{1}{4\pi} \left[\frac{e^{-jk\sqrt{(\xi - \xi')^2 + (y - y')^2}}}{\sqrt{(\xi - \xi')^2 + (y - y')^2}} - \frac{e^{-jk\sqrt{(\xi - \xi')^2 + (y - y')^2 + 4h^2}}}{\sqrt{(\xi - \xi')^2 + (y - y')^2 + 4h^2}} \right] \quad (57)$$

Although introduced initially in area 2, this function W can certainly be continued to all the other three areas in the $\xi - \xi'$ plane.

For the evaluation of Fourier transforms it is convenient to decompose Γ_D and Γ_H as follows:

$$\Gamma_D(\xi, \xi') = W(\xi - \xi') + U_D(\xi, \xi') \quad (58)$$

$$\Gamma_H(\xi, \xi') = W(\xi - \xi') + U_H(\xi, \xi')$$

By equation 56 the two functions U_D and U_H vanish identically in area 2. In the other three areas they are both expressible as a difference. Each of them has a very complicated form and will be written out in full in the appendix. The advantage of the decompositions in equations 58 lies in the fact that the dominant part W is relatively simple and continuous throughout the entire range of integration in the $\xi - \xi'$ plane. The discontinuities in Γ_D and Γ_H are left behind in U_D and U_H .

The Fourier transforms F_D and F_H of Γ_D and Γ_H have the following corresponding decompositions:

$$F_D(p, p') = w_D(p, p') + u_D(p, p') \quad (59)$$

$$F_H(p, p') = w_H(p, p') + u_H(p, p')$$

where

$$w_D(p, p') = \left(\frac{2}{\pi}\right)^2 \int_0^\infty d\xi \int_0^\infty d\xi' W(\xi - \xi') \sin p\xi \sin p'\xi' \quad (60)$$

$$w_H(p, p') = \left(\frac{2}{\pi}\right)^2 \int_0^\infty d\xi \int_0^\infty d\xi' W(\xi - \xi') \cos p\xi \cos p'\xi'$$

and

$$u_D(p, p') = \left(\frac{2}{\pi}\right)^2 \int_0^\infty d\xi \int_0^\infty d\xi' U_D(\xi, \xi') \sin p\xi \sin p'\xi' \quad (61)$$

$$u_H(p, p') = \left(\frac{2}{\pi}\right)^2 \int_0^\infty d\xi \int_0^\infty d\xi' U_H(\xi, \xi') \cos p\xi \cos p'\xi'$$

It will be shown below that both $w_D(p, p')$ and $w_H(p, p')$ contain a part proportional to $\delta(p - p')$.

The function $W(\xi - \xi')$, as defined in equation 57, can be converted to a form more suitable for Fourier transformation. This is achieved by applying the Fourier integral representation of the free-space Green's function given in equation 15. The integrand in equation 57 is essentially made up of free-space Green's functions. Expressing the integrand in equation 57 as a Fourier integral, one can immediately perform the y - and y' -integrations. The result is

$$W(\xi - \xi') = \frac{1}{(2\pi)^3} \int_{-\infty}^{\infty} d\alpha \int_{-\infty}^{\infty} d\beta \int_{-\infty}^{\infty} d\gamma \left(\frac{\sin \beta a}{\beta a}\right)^2 \frac{1 - e^{-j2\gamma h}}{\alpha^2 + \beta^2 + \gamma^2 - k^2} e^{-j\alpha(\xi - \xi')} \quad (62)$$

Furthermore, one can carry out the α -integration and obtain

$$W(\xi - \xi') = \frac{1}{8\pi^2 j} \int_{-\infty}^{\infty} d\beta \int_{-\infty}^{\infty} d\gamma \left(\frac{\sin \beta a}{\beta a}\right)^2 \frac{1 - e^{-j2\gamma h}}{\sqrt{k^2 - \beta^2 - \gamma^2}} e^{-j\sqrt{k^2 - \beta^2 - \gamma^2}|\xi - \xi'|} \quad (63)$$

where the square root is defined to make

$$\sqrt{k^2 - \beta^2 - \gamma^2} \rightarrow k \quad (64)$$

as k goes to ∞ . Equation 63 offers a more convenient representation of the function $W(\xi - \xi')$ than equation 57, since the ξ - and ξ' -dependences are all contained in a simple exponential function. The Fourier transform of W can be obtained by first calculating the Fourier transform of this exponential function.

Consider first the double Fourier sine transform. One can show by straightforward integration that

$$\int_0^{\infty} d\xi e^{-j\sqrt{k^2 - \beta^2 - \gamma^2}|\xi - \xi'|} \sin p\xi = \frac{-2j\sqrt{k^2 - \beta^2 - \gamma^2}}{k^2 - \beta^2 - \gamma^2 - p^2} \sin p\xi' - \frac{p}{k^2 - \beta^2 - \gamma^2 - p^2} e^{-j\sqrt{k^2 - \beta^2 - \gamma^2}\xi'} \quad (65)$$

In deriving this expression one must keep in mind that k has a small negative imaginary part, as indicated in equation 16, so that the integrand vanishes at infinity. Note especially that the right-hand side contains a term proportional to $\sin p\xi'$. Multiplying both sides of equation 65 by $\sin p'\xi'$ and integrating over ξ' from 0 to ∞ , one obtains explicitly the following double Fourier sine transform:

$$\int_0^{\infty} d\xi \int_0^{\infty} d\xi' e^{-j\sqrt{k^2 - \beta^2 - \gamma^2}|\xi - \xi'|} \sin p\xi \sin p'\xi' = -\pi j \frac{\sqrt{k^2 - \beta^2 - \gamma^2}}{k^2 - \beta^2 - \gamma^2 - p^2} \delta(p - p') + \frac{pp'}{(k^2 - \beta^2 - \gamma^2 - p^2)(k^2 - \beta^2 - \gamma^2 - p'^2)} \quad (66)$$

The δ -function comes about as a consequence of equations 47.

The double Fourier cosine transform can be evaluated in a similar way. The result is

$$\int_0^{\infty} d\xi \int_0^{\infty} d\xi' e^{-j\sqrt{k^2 - \beta^2 - \gamma^2}|\xi - \xi'|} \cos p\xi \cos p'\xi' = -\pi j \frac{\sqrt{k^2 - \beta^2 - \gamma^2}}{k^2 - \beta^2 - \gamma^2 - p^2} \delta(p - p') + \frac{k^2 - \beta^2 - \gamma^2}{(k^2 - \beta^2 - \gamma^2 - p^2)(k^2 - \beta^2 - \gamma^2 - p'^2)} \quad (67)$$

Note that the coefficient of the δ -function in equation 67 is the same as that in equation 66.

Having isolated the δ -function in the Fourier transforms in equations 66 and 67, one is in the position to write down explicit expressions for the functions $\rho(p)$ and $\Lambda(p,p')$ defined in equations 53 and 55. The result for $\rho(p)$ is

$$\rho(p) = \frac{1}{2\pi^3} \int_{-\infty}^{\infty} d\beta \int_{-\infty}^{\infty} d\gamma \left(\frac{\sin \beta a}{\beta a} \right)^2 \frac{1 - e^{-j2\gamma h}}{p^2 + \beta^2 + \gamma^2 - k^2} \quad (68)$$

The γ -integration can be further carried out, and one obtains

$$\rho(p) = \frac{1}{2\pi^2 j} \int_{-\infty}^{\infty} d\beta \left(\frac{\sin \beta a}{\beta a} \right)^2 \frac{1 - e^{-j2\sqrt{k^2 - p^2 - \beta^2} h}}{\sqrt{k^2 - p^2 - \beta^2}} \quad (69)$$

The result for $\Lambda(p,p')$ is

$$\begin{aligned} \Lambda(p,p') = & \frac{1}{2\pi^4 j} \int_{-\infty}^{\infty} d\beta \int_{-\infty}^{\infty} d\gamma \left(\frac{\sin \beta a}{\beta a} \right)^2 \frac{1 - e^{-j2\gamma h}}{\sqrt{k^2 - \beta^2 - \gamma^2}} \frac{k^2(k^2 - \beta^2 - \gamma^2) - p^2 p'^2}{(k^2 - \beta^2 - \gamma^2 - p^2)(k^2 - \beta^2 - \gamma^2 - p'^2)} \\ & + k^2 u_H(p,p') - pp' u_D(p,p') \end{aligned} \quad (70)$$

If one wishes, one can write out explicitly the two functions u_H and u_D with the help of equations 61 and the appendix. They are made up of a set of complicated four-dimensional integrals.

SECTION VIII

MODAL STRUCTURE OF EXCITATION

In this section the properties of the integral equation 54 will be examined. The findings will not only provide valuable qualitative information on the solution, but will also suggest the appropriate method for constructing an approximate solution.

A very common technique for solving an integral equation of the type of equation 54 is iteration. Using this technique one can immediately write down the following first-iterated solution:

$$A(p) \approx \frac{M(p)}{(k^2 - p^2) \rho(p)} \quad (71)$$

where

$$M(p) = - \frac{2j\omega\epsilon_0 V_0}{\pi^2} \left[1 - \int_0^\infty dp' \frac{\Lambda(p, p')}{(k^2 - p'^2) \rho(p')} \right] \quad (72)$$

Although this approximate solution is not expected to be very accurate, and will not be used in the quantitative calculations of this study, it does reveal many of the general properties of the true solution.

The behavior of the solution in equation 71 is dominated by the zeros of the denominator. These zeros give rise to infinities in $A(p)$. Each of the infinities corresponds to a discrete mode of electromagnetic propagation along the simulator structure in figure 2. Besides these discrete modes, which are infinite in number, the solution also exhibits a spectrum of continuous modes, as will be seen below.

The first two zeros of the denominator are easily found to be at $p = \pm k$. They correspond to the TEM mode of propagation. All the other zeros are contained in the function $\rho(p)$. Inasmuch as $\rho(p)$ is presented in the form of a definite integral in equation 69, these zeros are not as easy to locate accurately. For the purpose of a qualitative investigation, however, one can use an approximate evaluation of the integral. When the

half-width a of the rectangular strip can be considered large relative to the height h , the factor $(\sin \beta a / \beta a)^2$ in the integral in equation 69, as compared with the remainder, is sharply peaked at $\beta = 0$. As an approximation, one can replace the remainder by its value at $\beta = 0$, and obtain

$$\rho(p) \approx e^{-j\sqrt{k^2 - p^2} h} \frac{\sin(\sqrt{k^2 - p^2} h)}{\sqrt{k^2 - p^2}} \frac{1}{\pi^2} \int_{-\infty}^{\infty} d\beta \left(\frac{\sin \beta a}{\beta a} \right)^2 \quad (73)$$

The zeros of $\rho(p)$ in equation 73 are all contained in the factor $\sin(\sqrt{k^2 - p^2} h) / \sqrt{k^2 - p^2}$, which is an entire function of p . It has an infinite number of simple zeros located at

$$p = \pm \sqrt{k^2 - \left(\frac{n\pi}{h} \right)^2} \quad n = 1, 2, 3, \dots \quad (74)$$

Note that because of the square root in the denominator of the factor the case $n=0$ is not included. These values of p correspond to the propagation constants of the higher-order modes. They are seen to be either purely real or purely imaginary, implying thereby that some higher-order modes are unattenuated. However, if one had used equation 69 instead of the approximate equation 73 to compute the zeros, one would have obtained complex propagation constants. One would have concluded that all higher-order modes are more or less damped.

In addition to the zeros, $\rho(p)$ has branch points at $p = \pm k$, as the exponential factor in equation 73 shows. The branch cuts of $\rho(p)$ in the complex p -plane correspond to a continuous spectrum of propagation constants. The existence of continuous modes is typical of open waveguide structures.

Thus, based on the analytical properties of the denominator in equation 71, one concludes that the excitation on the simulator can be decomposed into certain discrete and continuous modes. One can show that these modes are in fact the propagation modes of an infinite, parallel-strip waveguide. The propagation constants of the lowest modes of this waveguide have been computed accurately in reference 4. The simple, approximate

formula for the higher-order propagation constants in equation 74 compares very well with the accurate values.

From these findings it is clear that the free term on the left-hand side of the integral equation 54 describes the properties of a parallel-strip waveguide. The role of the integral with kernel $\Lambda(p,p')$ is to bring into consideration other aspects of the simulator geometry. According to equation 70, Λ is made up of two parts. The first part is written out as a two-dimensional definite integral, and does not involve the linear dimension d of the triangular plates. Its occurrence in the kernel is a result of the fact that the simulator is a semi-infinite, rather than an infinite, waveguide. The second part of Λ in equation 70 involves the parameter d , and further elaborates the simulator geometry. It describes the fact that the simulator has a discontinuity in the form of a junction between a section of a conical waveguide and a parallel-strip waveguide. In equation 71 these effects of Λ enter in the numerator $M(p)$. They affect the amplitudes and phases of the modes which make up the complete solution.

SECTION IX

SELF-CONSISTENT SOLUTION

The recognition that the solution is made up of modes with well-defined propagation constants suggests a self-consistent method for solving the integral equation 54. In this method one first expresses the total current flowing on the simulator as a linear combination of the propagation modes of the parallel-strip waveguide. Each mode is represented by a simple exponential function of ξ involving a definite propagation constant. Such an expansion contains a number of unknown expansion coefficients. One then evaluates the Fourier cosine transform of this expression and substitutes it into the integral in equation 54 as a trial solution in place of the unknown function $A(p')$. The resulting equation can be solved for $A(p)$, and the solution is of the form in equation 71. As one has already seen, this solution itself is again a linear combination of the propagation modes of the parallel-strip waveguide. Consequently, the expansion coefficients can be determined self-consistently.

A self-consistent calculation can be performed with an arbitrary degree of elaborateness, depending on the number of expansion coefficients entered in the trial solution. In what follows, the integral equation 54 will be solved using the simplest self-consistent scheme. That is to say, the trial solution employed will involve only the TEM mode of propagation. In view of the geometry of the simulator and the manner in which it is excited, the current will be predominantly in the TEM mode. Hence, a TEM trial solution is expected to be satisfactory. One must emphasize, however, that this in no way means that the resulting solution exhibits only a TEM mode. It means simply that only the TEM component is determined self-consistently.

The current associated with the TEM mode is given by

$$I_{\text{TEM}}(\xi) = I_0 e^{-jk\xi} \quad (75)$$

where the amplitude I_0 is to be determined self-consistently. The Fourier cosine transform of the TEM current can be easily evaluated:

$$\frac{2}{\pi} \int_0^{\infty} d\xi I_{\text{TEM}}(\xi) \cos p\xi = \frac{2jk}{\pi} \frac{I_0}{p^2 - k^2} \quad (76)$$

on account of equation 16. Substituting the right-hand side of equation 76 into the integral of equation 54 as a trial solution for $A(p')$, one obtains the following approximate solution of the integral equation:

$$A(p) \approx \frac{N(p)}{(k^2 - p^2)\rho(p)} \quad (77)$$

where

$$N(p) = -\frac{2j\omega\epsilon_0 V_0}{\pi^2} - \frac{2jkI_0}{\pi} \int_0^{\infty} dp' \frac{\Lambda(p,p')}{p'^2 - k^2} \quad (78)$$

The total current is given by

$$I(\xi) = \int_0^{\infty} dp \frac{N(p)}{(k^2 - p^2)\rho(p)} \cos p\xi \quad (79)$$

This expression provides an approximate solution of the problem up to an unknown constant I_0 . One then determines this constant self-consistently by separating out the TEM part of $I(\xi)$ and substituting it into the left-hand side of equation 75.

It can be shown that both $N(p)$ and $\rho(p)$ are even functions of p , so that equation 79 can be rewritten as

$$I(\xi) = \frac{1}{2} \int_{-\infty}^{\infty} dp \frac{N(p)}{(k^2 - p^2)\rho(p)} e^{-jp\xi} \quad (80)$$

With $I(\xi)$ in this form one can evaluate the TEM part by the method of residues. The value of the integral is dependent on the singularities of the integrand

in the complex p -plane. As has been discussed in section VIII, the denominator of equation 80 gives rise to simple poles and branch cuts. They correspond to the discrete and continuous modes of the parallel-strip waveguide. These singularities are shown in figure 6. The singularities of the numerator $N(p)$, if any, need not be considered here.

The coordinate ξ is always positive. For ξ sufficiently large, the path of integration in equation 80 can be closed by a large semicircular arc in the lower half of the complex p -plane. Then the TEM part of $I(\xi)$ is given by the residue at the pole $p = k$:

$$I_{\text{TEM}}(\xi) = \frac{j\pi N(k)}{2kp(k)} e^{-jk\xi} \quad (81)$$

Substituting equation 81 into equation 75 and using equation 78 one can solve for I_o , and obtain

$$I_o = \frac{V_o}{\pi Z_o} \frac{1}{\rho(k) + \int_0^\infty dp' \frac{\Lambda(k, p')}{k^2 - p'^2}} \quad (82)$$

where

$$Z_o = \sqrt{\frac{\mu_o}{\epsilon_o}} \approx 377 \text{ ohms} \quad (83)$$

With the value of I_o determined, equation 80 becomes an explicit, approximate formula for the total current flowing on the simulator.

It is possible to improve systematically the accuracy of the solution by including more and more higher-order modes in the trial solution.

The physical content of the self-consistent solution in equation 82 can be more easily appreciated if one rewrites it in the following form:

$$I_o = \frac{V_o}{Z_1 + Z_2 + Z_3} \quad (84)$$

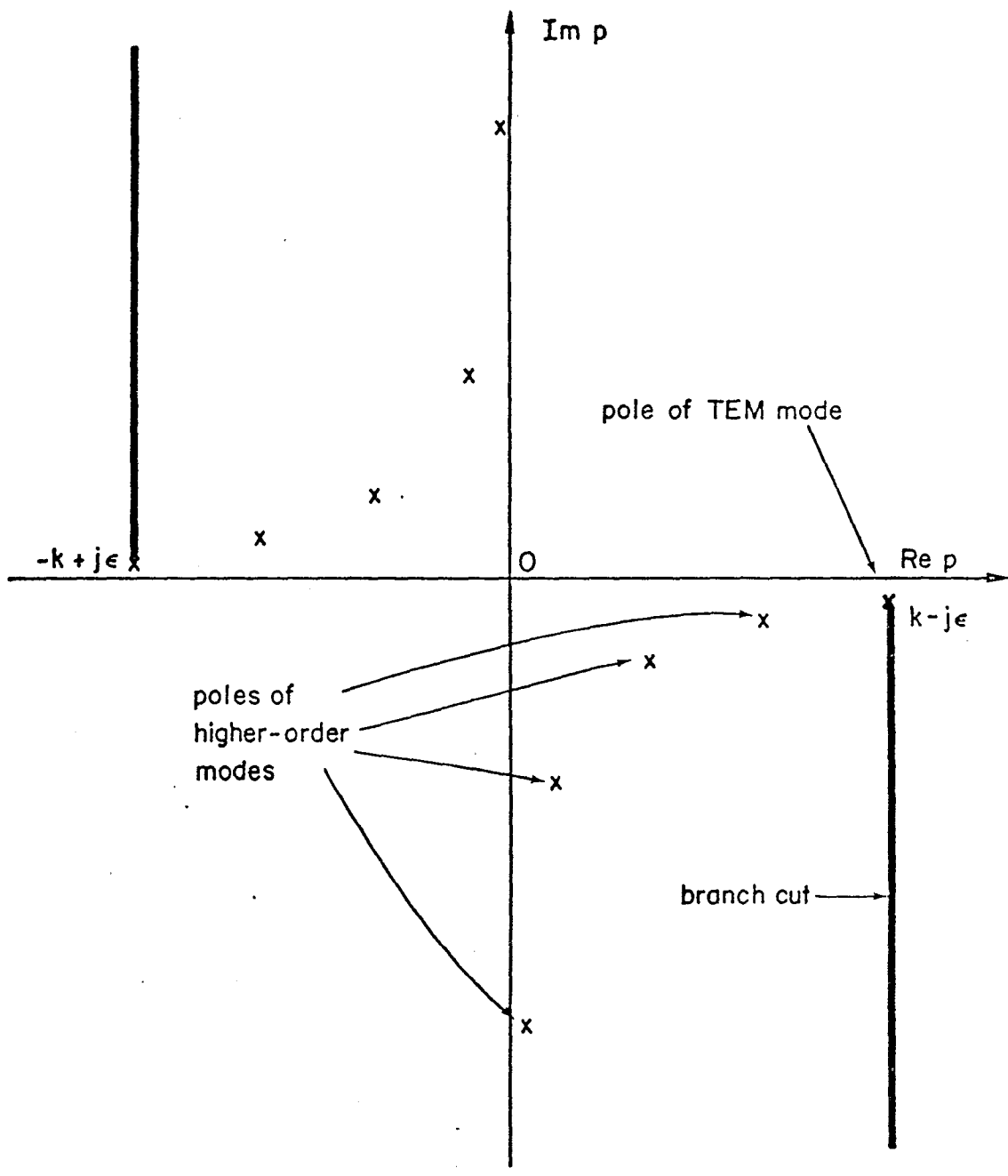


Figure 6. Singularities in the Complex p -Plane.

where Z_1 , Z_2 and Z_3 are three quantities with the dimension of an impedance. They are defined by

$$\begin{aligned} Z_1 &= \pi\rho(k)Z_0 \\ &= \frac{Z_0}{2\pi} \int_{-\infty}^{\infty} d\beta \left(\frac{\sin \beta a}{\beta a} \right)^2 \frac{1 - e^{-2|\beta|h}}{|\beta|} \end{aligned} \quad (85)$$

$$Z_2 = -\frac{kZ_0}{4\pi^2} \int_{-\infty}^{\infty} d\beta \left(\frac{\sin \beta a}{\beta a} \right)^2 \int_{-\infty}^{\infty} \frac{d\gamma}{\sqrt{k^2 - \beta^2 - \gamma^2}} \frac{1 - e^{-j2\gamma h}}{\beta^2 + \gamma^2} \quad (86)$$

and

$$Z_3 = \pi Z_0 \int_0^{\infty} dp' \frac{k^2 u_H(k, p') - kp' u_D(k, p')}{k^2 - p'^2} \quad (87)$$

Z_2 and Z_3 represent the integral of Λ in equation 82. Z_2 comes from that part of Λ that is expressed as a two-dimensional integral in equation 70, while Z_3 comes from the remainder. These impedances are functions of the three dimensionless parameters h/a , kh and d/h of the problem. It can be shown that Z_1 depends only on h/a , Z_2 depends on h/a and kh , and Z_3 depends on h/a , kh and d/h :

$$\begin{aligned} Z_1 &= Z_1 \left(\frac{h}{a} \right) \\ Z_2 &= Z_2 \left(\frac{h}{a}, kh \right) \\ Z_3 &= Z_3 \left(\frac{h}{a}, kh, \frac{d}{h} \right) \end{aligned} \quad (88)$$

Equation 84 interprets the TEM current I_0 as equivalent to that resulting from the application of a voltage V_0 across the terminals of three impedances Z_1 , Z_2 and Z_3 connected in series. The physical origin of these impedances can be traced among the findings of section VIII. Z_1 is the characteristic impedance of an infinite parallel-plate transmission line. Its expression

in equation 85 is of course not exact, but obtained under the approximation of averaging over the transverse direction. Z_2 is a correction to Z_1 , and takes account of the fact that the simulator model considered in this study has a semi-infinite, rather than infinite, structure. Z_3 is an equivalent impedance for the junction between the two different sections of the simulator, and embodies the effects of the junction discontinuity. It alone depends on the dimension d of the conical transmission line section.

The integral in equation 85 can be evaluated analytically. One obtains

$$Z_1 = \frac{2Z_0}{\pi} \left[\frac{h}{a} \tan^{-1} \left(\frac{a}{h} \right) + \frac{1}{4} \ln \left(\frac{h^2 + a^2}{a^2} \right) - \frac{1}{4} \left(\frac{h}{a} \right)^2 \ln \left(\frac{h^2 + a^2}{h^2} \right) \right] \quad (89)$$

and, with the help of equations 61, equation 87 can be rewritten as

$$Z_3 = 2jkZ_0 \int_0^\infty d\xi \int_0^\infty d\xi' \left[\cos k\xi U_H(\xi, \xi') - j \sin k\xi U_D(\xi, \xi') \right] e^{-jk\xi'} \quad (90)$$

where the functions U_H and U_D are provided in the appendix.

SECTION X

NUMERICAL RESULTS

This section presents the results of numerical calculations on the three impedances Z_1 , Z_2 and Z_3 . In these calculations the following sets of values of the three parameters in the problem are considered:

$$\frac{h}{a} = 1, 2, 3$$

$$kh = 0.1, 1, 10 \quad (91)$$

$$\frac{L}{h} = 2, 4, 8, 12, 16, 20$$

with

$$L = d \cos \theta \quad (92)$$

L can be regarded as the length of the conical transmission line section. The ratio d/h is related to L/h by the simple equation

$$\frac{d}{h} = \sqrt{\left(\frac{L}{h}\right)^2 + 1} \quad (93)$$

For a typical value of 50 meters for h , the three chosen values of kh in equation 91 correspond approximately to frequencies of 100 kHz, 1 MHz and 10 MHz, respectively.

The impedance Z_1 is purely real, and depends only on the ratio h/a . It can be computed easily from equation 89. The results are shown in table 1. As has been pointed out earlier in section IX, Z_1 is in fact the characteristic impedance of an infinite, parallel-plate transmission line. It has been investigated extensively by the method of conformal mapping in references 5 and 6. The numerical values of Z_1 obtained in reference 6 are quoted in table 1 for comparison. A glance at the table reveals that the two sets of impedance values calculated by the two totally

Table 1

VARIATION OF IMPEDANCE Z_1 WITH SEPARATION-TO-WIDTH RATIO h/a ($Z_0 = \sqrt{\mu_0/\epsilon_0} \approx 377$ OHMS)

$\frac{h}{a}$	Z_1/Z_0	
	From Equation 89	From Reference 6
1	0.50000	0.47264
2	0.70443	0.67116
3	0.83005	0.79525

different methods are in uniform, good agreement with each other. The difference is only about 5%. The agreement is also found to be equally good for values of h/a other than the three listed.

The numerical results for the impedance Z_2 are shown in table 2. It is seen that the real part of Z_2 is negative. But the combination $Z_1 + Z_2$, which can be regarded as the characteristic impedance of a semi-infinite parallel-plate transmission line, is passive as it should.

Table 3 shows the numerical results for the impedance Z_3 . They are obtained mostly for $kh = 0.1$. This is because, at higher values of kh , the integrand in equation 90 contains a large number of oscillations. The numerical calculation then becomes very time consuming. The table does include, however, two cases at $kh=1$ and 2.5 , and at values of h/a and L/h that are comparable to the dimensions of an existing simulator.

At $kh = 0.1$, table 3 shows that Z_3 is mainly imaginary. Its magnitude decreases with increasing L/h for all three values of h/a . Based on these data one can say that the transition across the junction is smoother the larger the ratio L/h becomes.

Table 2

VARIATION OF IMPEDANCE Z_2 WITH PARAMETERS kh AND h/a ($Z_0 = \sqrt{\mu_0/\epsilon_0} \approx 377$ OHMS)

kh	h/a	$\text{Re}(Z_2/Z_0)$	$\text{Im}(Z_2/Z_0)$
0.1	1	-0.00157	-0.0234
	2	-0.00157	-0.0269
	3	-0.00157	-0.0284
1	1	-0.127	-0.162
	2	-0.132	-0.203
	3	-0.133	-0.218
10	1	-0.246	-0.0163
	2	-0.344	-0.0311
	3	-0.404	-0.0440

Table 3

VARIATION OF IMPEDANCE Z_3 WITH
 PARAMETERS kh , h/a AND L/h ($Z_0 = \sqrt{\mu_0/\epsilon_0} \approx 377$ OHMS)

kh	$\frac{h}{a}$	$\frac{L}{h}$	$\text{Re } \frac{Z_3}{Z_0}$	$\text{Im } \frac{Z_3}{Z_0}$	
0.1	1	2	0.0028	0.035	
		4	0.0030	0.033	
		8	0.0030	0.029	
		12	0.0029	0.027	
		16	0.0028	0.026	
		20	0.0027	0.025	
	2	2	2	0.0028	0.040
			4	0.0030	0.037
			8	0.0030	0.034
			12	0.0029	0.032
			16	0.0028	0.031
			20	0.0026	0.030
	3	2	2	0.0028	0.042
			4	0.0030	0.039
			8	0.0030	0.036
			12	0.0028	0.034
			16	0.0027	0.033
			20	0.0026	0.032
	1.0	3	4	0.18	0.27
	2.5	3	4	0.47	0.20

SECTION XI

DISCUSSIONS

In this study one has succeeded in obtaining an approximate analytical formula for the total electric current flowing on a parallel-plate EMP simulator. This formula enables one to examine both qualitatively and quantitatively the nature of the excitation on the simulator. Contacts with previous work on different aspects of the simulator have been established. The formula, however, cannot yield directly the electromagnetic fields in the simulator's test volume. In order to determine the field components one will have to make further approximations.

One approximation consists of synthesizing the fields in the parallel-plate region from the field patterns of the discrete modes of an infinite, parallel-plate waveguide. These field patterns have been calculated in reference 4. The fields in the parallel-plate region can be expanded in terms of these patterns. It remains to determine the expansion coefficients. As an approximation the coefficients can be taken as identical to the expansion coefficients of the total current in terms of the model currents. That is to day, they are given by the residues of the integrand in equation 80 at the poles in the complex p -plane corresponding to the discrete waveguide modes.

Another method consists of constructing approximately an expression for the surface current density from that for the total current in equation 80. The variation of the surface current density on the simulator in the transverse direction is largely determined by the edge condition. One can distribute the total longitudinal current across the breadth of the simulator according to some simple analytical function which satisfies the edge condition. The electromagnetic fields can then be obtained from the surface current density by integration.

REFERENCES

- [1] Marin, L., "Modes on a Finite-Width, Parallel-Plate Simulator: I. Narrow Plates," Sensor and Simulation Notes, Note 201, Air Force Weapons Laboratory, Kirtland Air Force Base, NM, September 1974.
- [2] Marin, L., "Modes on a Finite-Width, Parallel-Plate Simulator: II. Wide Plates," Sensor and Simulation Notes, Note 223, Air Force Weapons Laboratory, Kirtland Air Force Base, NM, March 1977.
- [3] Yang, F.C. and L. Marin, "Field Distributions on a Two-Conical-Plate and a Curved Cylindrical-Plate Transmission Line," Sensor and Simulation Notes, Note 229, Air Force Weapons Laboratory, Kirtland Air Force Base, NM, September 1977.
- [4] Yang, F.C., "Discrete and Continuous Spectra of Finite-Width, Parallel-Plate Simulator's Fields," Sensor and Simulation Notes, Note 262, June 1979.
- [5] Baum, C.E., "Impedances and Field Distributions for Parallel Plate Transmission Line Simulators," Sensor and Simulation Notes, Note 21, Air Force Weapons Laboratory, Kirtland Air Force Base, NM, June 1966.
- [6] Brown, T.L. and K.D. Granzow, "A Parameter Study of Two Parallel Plate Transmission Line Simulators of EMP Sensor and Simulation Note 21," Sensor and Simulation Notes, Note 52, Air Force Weapons Laboratory, Kirtland Air Force Base, NM, April 1968.

APPENDIX

FUNCTIONS $U_D(\xi, \xi')$ AND $U_H(\xi, \xi')$

The functions $U_D(\xi, \xi')$ and $U_H(\xi, \xi')$ first occur in equations 58. They can be calculated from the relations

$$U_D(\xi, \xi') = \Gamma_D(\xi, \xi') - W(\xi - \xi') \quad (A1)$$

$$U_H(\xi, \xi') = \Gamma_H(\xi, \xi') - W(\xi - \xi')$$

Γ_D and Γ_H are certain averages of the Green's functions G_D and G_H defined in equations 14, 31, 32 and 33, while W is given in equations 56 and 57.

U_D and U_H have different forms in the four different areas of the $\xi - \xi'$ plane shown in figure 5:

1. In area 1 ($0 < \xi, \xi' < d$) one has

$$G_D(\xi, y, \xi', y') = \frac{1}{4\pi} \left[\frac{e^{-jk\sqrt{(\xi - \xi')^2 + (y - y')^2}}}{\sqrt{(\xi - \xi')^2 + (y - y')^2}} - \frac{e^{-jk\sqrt{\xi^2 + \xi'^2 - 2\xi\xi'\cos 2\theta + (y - y')^2}}}{\sqrt{\xi^2 + \xi'^2 - 2\xi\xi'\cos 2\theta + (y - y')^2}} \right]$$

$$G_H(\xi, y, \xi', y') = \frac{1}{4\pi} \left[\frac{e^{-jk\sqrt{(\xi - \xi')^2 + (y - y')^2}}}{\sqrt{(\xi - \xi')^2 + (y - y')^2}} - \cos 2\theta \frac{e^{-jk\sqrt{\xi^2 + \xi'^2 - 2\xi\xi'\cos 2\theta + (y - y')^2}}}{\sqrt{\xi^2 + \xi'^2 - 2\xi\xi'\cos 2\theta + (y - y')^2}} \right] \quad (A2)$$

Then

$$U_D(\xi, \xi') = \frac{d^2}{4a^2 \xi \xi'} \int_{-a\xi/d}^{a\xi/d} dy \int_{-a\xi'/d}^{a\xi'/d} dy' G_D(\xi, y, \xi', y') - W(\xi - \xi') \quad (A3)$$

$$U_H(\xi, \xi') = \frac{d^2}{4a^2 \xi \xi'} \int_{-a\xi/d}^{a\xi/d} dy \int_{-a\xi'/d}^{a\xi'/d} dy' G_H(\xi, y, \xi', y') - W(\xi - \xi')$$

2. In area 2 ($d < \xi, \xi' < \infty$) one has, by equation 56,

$$U_D(\xi, \xi') = 0 \quad (A4)$$

$$U_H(\xi, \xi') = 0$$

3. In area 3 ($0 < \xi < d, d < \xi' < \infty$) one has

$$G_D(\xi, y, \xi', y') = \frac{1}{4\pi} \left[\frac{e^{-jk\sqrt{(\xi \cos \theta - \xi' + d - d \cos \theta)^2 + (y - y')^2 + (\xi \sin \theta - h)^2}}}{\sqrt{(\xi \cos \theta - \xi' + d - d \cos \theta)^2 + (y - y')^2 + (\xi \sin \theta - h)^2}} - \frac{e^{-jk\sqrt{(\xi \cos \theta - \xi' + d - d \cos \theta)^2 + (y - y')^2 + (\xi \sin \theta + h)^2}}}{\sqrt{(\xi \cos \theta - \xi' + d - d \cos \theta)^2 + (y - y')^2 + (\xi \sin \theta + h)^2}} \right]$$

$$G_H(\xi, y, \xi', y') = \cos \theta G_D(\xi, y, \xi', y') \quad (A5)$$

Then

$$U_D(\xi, \xi') = \frac{d}{4a^2 \xi} \int_{-a\xi/d}^{a\xi/d} dy \int_{-a}^a dy' G_D(\xi, y, \xi', y') - W(\xi - \xi') \quad (A6)$$

$$U_H(\xi, \xi') = \frac{d}{4a^2 \xi} \int_{-a\xi/d}^{a\xi/d} dy \int_{-a}^a dy' G_H(\xi, y, \xi', y') - W(\xi - \xi')$$

4. In area 4 ($d < \xi < \infty$, $0 < \xi' < d$) one has

$$G_D(\xi, y, \xi', y') = \frac{1}{4\pi} \left[\frac{e^{-jk\sqrt{(\xi-d+d\cos\theta-\xi'\cos\theta)^2 + (y-y')^2 + (h-\xi'\sin\theta)^2}}{\sqrt{(\xi-d+d\cos\theta-\xi'\cos\theta)^2 + (y-y')^2 + (h-\xi'\sin\theta)^2}} - \frac{e^{-jk\sqrt{(\xi-d+d\cos\theta-\xi'\cos\theta)^2 + (y-y')^2 + (h+\xi'\sin\theta)^2}}{\sqrt{(\xi-d+d\cos\theta-\xi'\cos\theta)^2 + (y-y')^2 + (h+\xi'\sin\theta)^2}} \right]$$

$$G_H(\xi, y, \xi', y') = \cos\theta G_D(\xi, y, \xi', y') \quad (A7)$$

Then

$$U_D(\xi, \xi') = \frac{d}{4a^2\xi'} \int_{-a}^a dy \int_{-a\xi'/d}^{a\xi'/d} dy' G_D(\xi, y, \xi', y') - W(\xi - \xi') \quad (A8)$$

$$U_H(\xi, \xi') = \frac{d}{4a^2\xi'} \int_{-a}^a dy \int_{-a\xi'/d}^{a\xi'/d} dy' G_H(\xi, y, \xi', y') - W(\xi - \xi')$$

Note that the forms of $U_D(\xi, \xi')$ and $U_H(\xi, \xi')$ in area 4 are obtainable from those in area 3 by interchanging the variables ξ and ξ' .